THE JOURNAL OF BIOLOGICAL CHEMISTRY VOL. 286, NO. 34, pp. 30087–30096, August 26, 2011

Mechanism of Actin Filament Bundling by Fascin*[S]

Received for publication, April 14, 2011, and in revised form, June 14, 2011 Published, JBC Papers in Press, June 18, 2011, DOI 10.1074/jbc.M111.251439

Silvia Jansen[‡], Agnieszka Collins[§], Changsong Yang[§], Grzegorz Rebowski[‡], Tatyana Svitkina[§1], and Roberto Dominguez[‡2]

From the [‡]Department of Physiology, University of Pennsylvania School of Medicine, and the [§]Department of Biology, University of Pennsylvania, Philadelphia, Pennsylvania 19104

Fascin is the main actin filament bundling protein in filopodia. Because of the important role filopodia play in cell migration, fascin is emerging as a major target for cancer drug discovery. However, an understanding of the mechanism of bundle formation by fascin is critically lacking. Fascin consists of four β-trefoil domains. Here, we show that fascin contains two major actin-binding sites, coinciding with regions of high sequence conservation in β-trefoil domains 1 and 3. The site in β-trefoil-1 is located near the binding site of the fascin inhibitor macroketone and comprises residue Ser-39, whose phosphorylation by protein kinase C down-regulates actin bundling and formation of filopodia. The site in β-trefoil-3 is related by pseudo-2-fold symmetry to that in β-trefoil-1. The two sites are ~5 nm apart, resulting in a distance between actin filaments in the bundle of ~8.1 nm. Residue mutations in both sites disrupt bundle formation *in vitro* as assessed by co-sedimentation with actin and electron microscopy and severely impair formation of filopodia in cells as determined by rescue experiments in fascin-depleted cells. Mutations of other areas of the fascin surface also affect actin bundling and formation of filopodia albeit to a lesser extent, suggesting that, in addition to the two major actin-binding sites, fascin makes secondary contacts with other filaments in the bundle. In a high resolution crystal structure of fascin, molecules of glycerol and polyethylene glycol are bound in pockets located within the two major actin-binding sites. These molecules could guide the rational design of new anticancer fascin inhibitors.

Fascin is the major actin filament (F-actin) bundling protein in protrusive cellular structures such as filopodia, dendrites, and invadopodia that play critical roles in cell motility, guidance, and invasion of the extracellular matrix (1–3). Fascin expression is up-regulated in various types of cancers, including lymphomas, glioblastomas, and carcinomas, where its overexpression correlates with increased tumor metastasis and invasiveness (4). As a result, fascin is used as a marker in cancer diagnosis and prognosis and is also emerging as an attractive target in cancer drug discovery (1, 5). The development of such therapeutic applications requires a thorough understanding of the molecular mechanism of F-actin bundling by fascin. An important step in this direction was the recent description of crystal structures of fascin, including that of a complex of fascin with the antimetastatic agent macroketone (5, 6). The 55-kDa fascin polypeptide folds into four β-trefoil domains with domains 1-2 and 3-4 forming two semi-independent units related by pseudo-2-fold symmetry. The binding site of macroketone is located in β-trefoil-4 near Ser^{39} in β-trefoil-1 whose phosphorylation by protein kinase C (PKC) inhibits actin bundling by fascin (7). Ser^{39} is also part of a sequence motif (^{29}FGFKVNASASSLKKK^{43}) that shows similarity with an actin-binding site of another PKC substrate, myristoylated alanine-rich protein kinase C substrate (MARCKS)[3] (8). Based on these observations, it is thought that the area surrounding Ser^{39} near the interface between β-trefoil domains 1 and 4 harbors one of the actin-binding sites of fascin. However, this has not been demonstrated conclusively. Moreover, since its discovery, fascin was shown to be monomeric (9), implying that it must contain at least one more actin-binding site to account for its F-actin bundling activity. In accord with this notion, limited proteolysis indicated that a second actin-binding site could be contained within the fragment 277–493, encompassing most of β-trefoil domains 3 and 4 (7). Mutagenesis screening in the *Drosophila* fascin homolog *singed* further identified two amino acids, Ser^{289} in β-trefoil-3 and Gly^{409} in β-trefoil-4 (corresponding to Ser^{274} and Gly^{396} in human fascin), that when mutated produce severe kinked bristle phenotypes (10). However, these two studies predate the determination of the crystal structure of fascin. In the structure, Ser^{274} and Gly^{396} are mostly buried, whereas the fragment 277–493 lacks one of the β-strands of β-trefoil-3 such that in both cases folding might have been compromised. Thus, our knowledge of the exact location and disposition of the actin-binding sites within the three-dimensional structure of fascin is unsatisfactory, and the mechanism of bundle formation is not well understood. Based on a high resolution crystal structure of fascin, structure-guided mutagenesis, and biochemical and cellular studies, we show here that fascin contains two major actin-binding sites,

* This work was supported, in whole or in part, by National Institutes of Health Grants MH087950 and HL086655 (to R. D.) and GM070898 (to T. S.). This work was also supported by a fellowship from the Research Foundation of Flanders (to S. J.).

[S] The on-line version of this article (available at http://www.jbc.org) contains supplemental Movie 1 and Figs. 1–6.

The atomic coordinates and structure factors (code 3P53) have been deposited in the Protein Data Bank, Research Collaboratory for Structural Bioinformatics, Rutgers University, New Brunswick, NJ (http://www.rcsb.org/).

[1] To whom correspondence may be addressed: Dept. of Biology, 221 Leidy Laboratories, University of Pennsylvania, 3740 Hamilton Walk, Philadelphia, PA 19104. Tel.: 215-898-5736; Fax: 215-898-8780; E-mail: svitkina@sas.upenn.edu.

[2] To whom correspondence may be addressed: Dept. of Physiology, A-507 Richards Bldg., University of Pennsylvania School of Medicine, 3700 Hamilton Walk, Philadelphia, PA 19104. Tel.: 215-573-4559; Fax: 215-573-5851; E-mail: droberto@mail.med.upenn.edu.

[3] The abbreviation used is: MARCKS, myristoylated alanine-rich protein kinase C substrate.

coinciding with areas of high sequence conservation in β-trefoil domains 1 and 3.

EXPERIMENTAL PROCEDURES

Proteins—The cDNA encoding for human fascin-1 was purchased from American Type Culture Collection (clone MGC-3899) and cloned between the NdeI and EcoRI sites of vector pTYB12 (New England Biolabs). Point mutations were generated using the QuikChange mutagenesis kit (Agilent). Cells were grown in Terrific Broth medium at 37 °C to an A_{600} of 1.0–1.2. Expression was induced with addition of 0.5 mM isopropyl β-D-thiogalactopyranoside for 16 h at 20 °C. Cells were resuspended in chitin column equilibration buffer (20 mM Tris-HCl, pH 8.0, 500 mM NaCl, 1 mM EDTA, 1 mM PMSF) and purified through a chitin affinity column followed by purification on a Mono Q ion exchange column (GE Healthcare) using a 40–500 mM NaCl gradient in 20 mM Tris (pH 8.0), 1 mM DTT. Se-Met substituted fascin was obtained by growing cells in SelenoMet medium (Athena Enzyme Systems) supplemented with 70 mg/ml selenomethionine (Acros Organics). Actin was purified from rabbit skeletal muscle as described (11).

Crystallization, Data Collection, and Structure Determination—Fascin was dialyzed against 20 mM Tris-HCl, pH 8.0, 100 mM NaCl, 5 mM DTT and concentrated to 10 mg/ml using a Vivaspin centrifugal device (Sartorius Stedim Biotech). Crystals of wild type and Se-Met substituted fascin were obtained by optimization of previously reported conditions (Protein Data Bank code 1DFC) using the hanging drop vapor diffusion method at 20 °C. A typical 2-μl drop consisted of a 1:1 (v/v) mixture of protein solution and a well solution containing 0.2 M lithium acetate dihydrate, 20–24% polyethylene glycol (PEG) 3500, and 4% glycerol. Crystals were flash frozen in liquid nitrogen after a short passage through a solution containing 20% glycerol added to the crystallization buffer.

X-ray data sets were collected from wild type and Se-Met-substituted crystals (Table 1) using beamline 17-ID of the Industrial Macromolecular Crystallography Association-Collaborative Access Team at the Advance Photon Source (Argonne, IL). Data indexing and scaling were performed with the program HKL2000 (HKL Research Inc.). The structure was determined using a combination of molecular replacement and single wavelength anomalous diffraction phasing as implemented in the subroutine AutoSol of the program Phenix (12). Model building and refinement were performed with the programs Coot (13) and Phenix. Illustrations were prepared with the program PyMOL (Schrödinger, LLC).

Sedimentation (Pelleting) Assay—Actin (25 μM) in G-buffer (2 mM Tris, pH 7.4, 0.2 mM $CaCl_2$, 0.2 mM ATP, 1 mM DTT, 1 mM NaN_3) was polymerized with addition of 50 mM KCl, 2 mM $MgCl_2$, and 1 mM ATP for 7 min at room temperature. Fascin constructs were first centrifuged at 224,000 × *g* for 30 min to remove potential aggregates. F-actin (15 μM) was incubated with 15 μM fascin constructs overnight at room temperature. Samples were centrifuged for 30 min at two different speeds, 10,000 × *g* (for bundling experiments) and 224,000 × *g* (for binding experiments). Equal volumes of supernatant and pellet were analyzed by 8.5% SDS-PAGE.

EM Analysis of Fascin-Actin Bundles—For EM visualization, actin at 25 μM was polymerized as above. Bundles were prepared by mixing prepolymerized actin with wild type or mutant fascin at a 1:1 molar ratio and incubating overnight. The samples were then diluted to 1 μM in F-buffer (100 mM NaCl, 2 mM $MgCl_2$, 1 mM NaN_3, 0.2 mM EGTA, 1 mM DTT, 5 mM PIPES, pH.7.6) and applied to Formvar- and carbon-coated 200 mesh copper grids. The samples were adsorbed onto grids for 30 s, blotted to remove excess solution, negatively stained with 1% (w/v) uranyl acetate for 1 min, blotted, and dried. The EM study of actin filaments and fascin-actin bundles was performed on a JEM-1011 transmission electron microscope (JEOL) at an accelerating voltage of 100 kV and a magnification of 40,000× or 100,000×. Images were captured on an Orius 835.10W charge-coupled device camera (Gatan). Bundle parameters, including width, interfilament distance, and the number of filaments per bundle, were measured using the Linescan tool of the MetaMorph imaging software (Molecular Devices). The intensity profile along a line drawn across a bundle showed a series of peaks corresponding to the number of filaments in the bundle. The distance between peaks in the intensity profiles was taken as the distance between filament centers. Two-dimensional bundles in which all the actin filaments were in the same plane (known as rafts) were selected for determination of interfilament distances to circumvent typical problems encountered with the study of three-dimensional bundles such as disorder and polymorphism (14). The two-dimensionality of the bundles was confirmed by analysis of tilted images at ±20°. For each fascin construct, 10 or more bundles were analyzed. Statistical analyses were performed using Student's *t* test with the program Excel (Microsoft).

Cell Culture, Transfection, and Microscopy—A fascin knockdown was generated as described (3) by transfecting mouse melanoma B16-F1 cultured cells (15) with shRNA construct pC-SUPER-fascin-Tm that targets nucleotides 741–759 of mouse fascin-1 (GenBank™ accession number NM_007984). Cyan fluorescent protein was expressed under a different promoter to allow for the visualization of transfected cells. Transfection of 1-day-old cultures (day 1) of B16-F1 cells at 60–80% confluence was performed using Lipofectamine LTX and Plus reagents (Invitrogen) according to the manufacturer's protocol. The following day (day 2), cells were replated and cultured overnight. On day 3, cells were transfected with rescue constructs (GFP vector or GFP-tagged human fascin constructs refractory to RNAi). On day 4, cells were transferred onto laminin-coated glass coverslips and cultured for 3 days. On day 7 (6 days after the transfection with shRNA), cells were fixed with 4% formaldehyde in PBS for 20 min, permeabilized with 1% Triton X-100 in PBS for 5 min, and stained with Alexa Fluor 594-phalloidin for 30 min. Samples were analyzed using an inverted microscope (Eclipse TE2000, Nikon) equipped with a Plan Apo 100× numerical aperture 1.3 objective (Nikon) and a Cascade 512B charge-coupled device camera (Roper Scientific) driven by the MetaMorph Imaging software (Molecular Devices). For the quantification of filopodia, pC-SUPER-fascin-Tm-positive cells were identified in the cyan fluorescent protein channel, and GFP-fascin signals were imaged in the yellow fluorescent protein channel. Filopodia were counted based on

yellow fluorescent protein intensity or filamentous actin staining. Only the bundles that showed 1.2 or higher fluorescence intensity above the local background were included.

TABLE 1

Crystallographic data, phasing, and refinement statistics

Values in parentheses correspond to highest resolution shell. FOM, figure of merit; r.m.s.d., root mean square deviation.

	Native	Selenium peak
Diffraction data		
Wavelength (Å)	1.0	0.9795
Space group	C 2	C 2
Unit cell *a*, *b*, *c* (Å)	161.7, 71.0, 112.7	161.1, 70.8, 113.1
Unit cell α, β, γ (°)	90.0, 131.23, 90.0	90.0, 131.46, 90.0
Resolution (Å)	2.0-30.7 (2.0-2.07)	3.2-43.0 (3.2-3.3)
Completeness (%)	98.1 (87.3)	94.3 (82.1)
Multiplicity	6.9 (4.4)	7.4 (5.4)
R_{merge} [a] (%)	5.7 (46.2)	5.0 (18.1)
I/σ	22.5 (2.6)	28.7 (9.8)
Phasing		
Number of selenium sites		6
FOM, anomalous only		0.47
FOM, density modification		0.71
Refinement		
Resolution (Å)	2.0-30.7 (2.05-2.0)	
No. of reflections	63,704	
Completeness (%)	97.9 (84.0)	
No. of residues/waters	970/396	
R_{factor} [b] (%)	17.8 (27.7)	
R_{free} [c] (%)	22.0 (34.4)	
r.m.s.d. bonds (Å)	0.007	
r.m.s.d. angles (°)	1.0	
B-factor protein (Å^2)	43.9	
B-factor solvent (Å^2)	44.6	
Protein Data Bank code	3P53	

[a] $R_{merge} = \Sigma_{hkl}(I - I)/\Sigma I$ where I and I are the observed and mean intensities, respectively, of all observations of reflection *hkl*, including its symmetry-related equivalents.

[b] $R_{factor} = \Sigma_{hkl}||F_{obs}| - |F_{calc}||/\Sigma|F_{obs}|$ where F_{obs} and F_{calc} are the observed and calculated structure factors, respectively, of reflection *hkl*.

[c] R_{free}, R_{factor} calculated for a randomly selected subset of the reflections (5%) that were omitted during refinement.

RESULTS

Crystal Structure of Fascin—As a first step toward identifying the actin-binding sites on the surface of the fascin molecule, we turned to its crystal structure. A recently described crystal structure of fascin (6) had been deposited in the Protein Data Bank approximately 10 years ago (Protein Data Bank code 1DFC). Based on this original work, two additional structures of fascin were recently reported (5), alone and in complex with macroketone (Protein Data Bank codes 3LLP and 3O8K). The reported structures, however, lacked numerous surface loops, limiting our ability to perform a careful analysis of the fascin surface to identify potential actin-binding sites. By optimizing the original crystallization conditions and combining molecular replacement phases with experimental phases from a Se-Met derivative (see "Experimental Procedures" and Table 1), we obtained a 2.0-Å-resolution structure of fascin that comprises all the surface loops (Fig. 1 and supplemental Movie 1). The asymmetric unit contains two fascin molecules. Molecule A is well defined in the electron density map, except for the first seven N-terminal residues. Molecule B lacks five residues at the N terminus and four residues of one of the loops (^{52}PDEA^{55}). The surface of the fascin molecule is irregular, displaying many cavities and grooves, which in the current structure are occupied by solvent molecules and compounds used in crystallization and freezing such as fragments of polyethylene glycol and molecules of glycerol (Fig. 1). As we explain below, the serendipitous occurrence of some these compounds within the actin-binding sites of the fascin molecule opens new opportunities for the rational design of fascin inhibitors. A large groove separates the four β-trefoil domains into two pairs (1-2 and 3-4) disposed in a V-shape with respect to one another (supplemental Fig. 1). A comparison of the two molecules of the

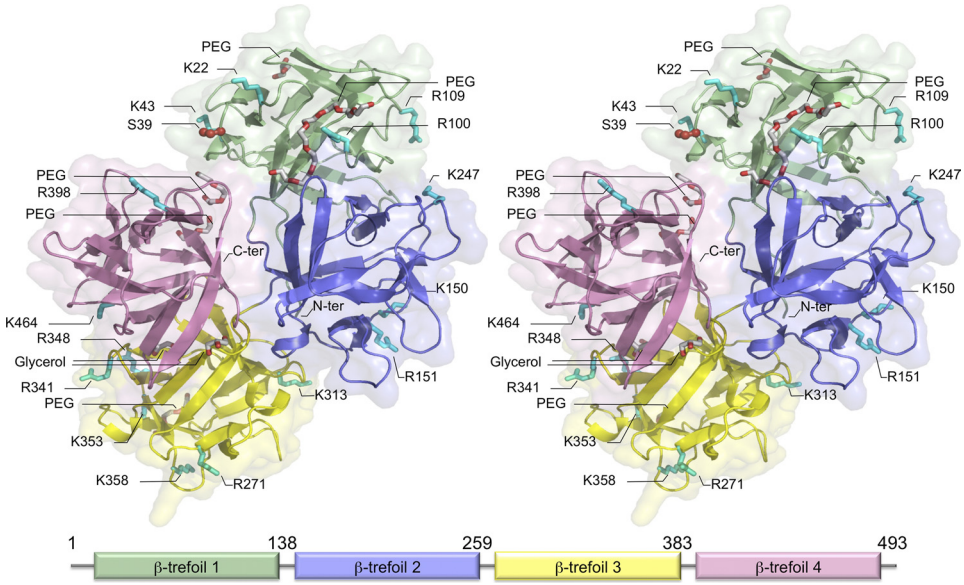

FIGURE 1. **Structure of fascin and amino acids mutated in this study.** Wall-eyed stereo diagram of the 2.0-Å-resolution crystal structure of fascin, showing ribbon and surface representations. There are two fascin molecules in the asymmetric unit of the crystal; only molecule A is shown. The four β-trefoil domains are highlighted with different colors as indicated by the diagram at the *bottom* of the figure. Also shown are the side chains of residues mutated in this study (*cyan*), molecules of glycerol and PEG bound in the structure, and Ser^{39} (*red*), which is phosphorylated by PKC. Note that a large groove effectively separates the four β-trefoil domains into two pairs, 1-2 and 3-4. Inter-β-trefoil domain contacts are more extensive within pairs (see also supplemental Fig. 1 and supplemental Movie 1). *N-ter*, N terminus; *C-ter*, C terminus.

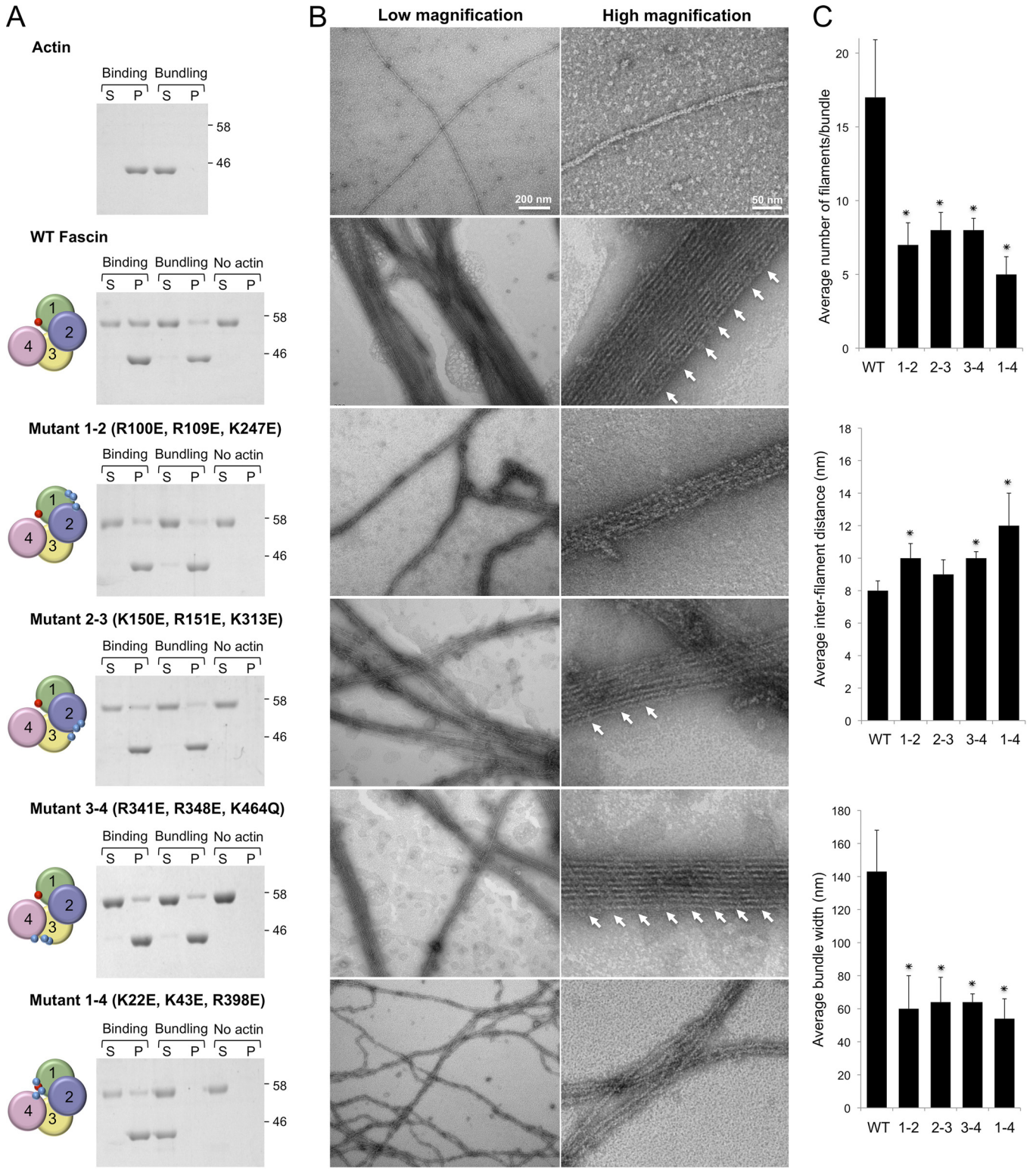

FIGURE 2. **Actin binding and bundling activities of wild type and mutant fascin.** *A*, results of binding (high speed; 224,000 × *g*) and bundling (low speed; 10,000 × *g*) co-sedimentation (pelleting) assays with filamentous F-actin, including control experiments (actin and fascin alone). Supernatant (*S*) and pellet (*P*) fractions were analyzed by gel electrophoresis. Also shown is a description of the mutants, including specific amino acids substituted in each mutant and schematic representations of their locations in the structure (β-trefoil domains colored according to Fig. 1; mutated residues and Ser^{39} represented by *blue balls* and a *red ball*, respectively). Mutants are named according to the numbers of the β-trefoil domains that were mutated in each case. *B*, representative transmission electron micrographs of negatively stained actin filaments alone and in the presence of wild type or mutant fascin (aligned with *A*). Low magnification images (*left*; *scale bar*, 200 nm) show that nearly all the actin filaments are incorporated into bundles in the presence of wild type fascin or fascin mutants. High magnification images (*right*; *scale bar*, 50 nm) show examples of a thick ordered bundle with periodic striations (indicated by *arrows*) formed by wild type fascin and thinner bundles with aberrant morphology formed by the fascin mutants. The bundles formed by mutants 2-3 and 3-4 often show striations (indicated by *arrows*). *C*, quantitative analysis of the bundles formed in the presence of wild type and mutant fascin ($n = 10$). *Asterisks* indicate statistically significant differences relative to wild type fascin ($p < 0.02$). *Error bars*, S.D.

asymmetric unit reveals that extensive interdomain interactions keep the relative position of β-trefoil domains within pairs mostly unchanged (Cα root mean square deviation of 0.56 and 0.47 Å between pairs 1-2 and 3-4, respectively). In contrast, the orientation of the pairs with respect to each other varies more significantly, resulting in an overall Cα root mean square deviation of 1.2 Å between the two molecules of the asymmetric unit.

Mapping the Actin-binding Sites by Structure-guided Mutagenesis—The architecture of the fascin molecule suggested that each pair of β-trefoil domains could function semi-independently and could thus each harbor an actin-binding site. Because of the pseudo-2-fold symmetry of the pairs, one possibility was that the actin-binding sites would be located at the interface between β-trefoil domains. To test this possibility, we made triple mutants targeting well separated, surface-exposed residues at the interface between β-trefoil domains 1-2 and 3-4 as well as 2-3 and 1-4 (as a control). Because the surface of the actin filament is mostly negatively charged, we targeted for mutagenesis positively charged amino acids (Lys and Arg) on the surface of the fascin molecule, which were replaced by glutamate to interfere with potential electrostatic interactions (see Figs. 1*A* and 2*A* for a detailed description of the mutants and their location in the structure). The mutants were named 1-2, 2-3, 3-4, and 1-4 according to the numbers of the β-trefoil domains that were mutated in each case. With the exception of mutant 3-4, the circular dichroism spectra of the mutants aligned well with that of wild type fascin (supplemental Fig. 2), indicating that the mutated proteins were properly folded. The spectrum of mutant 3-4 was slightly shifted, possibly due to the breakage of a salt bridge linking β-trefoil domains 3 and 4 between residues Lys^{464} (mutated) and Asp^{342}. Nevertheless, this mutant retained strong bundling activity *in vitro* (see below), suggesting that it was properly folded.

The actin binding and bundling activities of the fascin mutants were first assessed using high speed (224,000 × *g*) and low speed (10,000 × *g*) co-sedimentation with F-actin, respectively (Fig. 2*A*). All the mutants seemed to bind actin similarly to wild type fascin. In contrast, their bundling activities varied; mutant 1-4 did not appear to bundle actin, mutant 1-2 showed somewhat reduced bundling activity, and mutants 2-3 and 3-4 showed actin bundling activities comparable with that of wild type fascin. This assay, however, could not reveal whether these bundles were properly formed.

Negative staining EM was used to investigate the morphology of the bundles (Fig. 2*B*). In the absence of fascin, the actin filaments did not form bundles, whereas filaments incubated overnight with wild type fascin formed parallel bundles. As determined by decoration with myosin subfragment 1, the fascin-actin bundles had well defined polarity, *i.e.* all the filaments in a bundle had the same orientation (supplemental Fig. 3). The bundles formed by wild type fascin had an average width of ~142 nm and contained ~17 filaments (Fig. 2*C* and Table 2). For simplicity, the interfilament distance was determined using bundles in which all the actin filaments were in the same plane (rafts) as confirmed by analysis of tilted images at ±20° (supplemental Fig. 4), resulting in an apparent separation between filaments of ~8.1 nm (Fig. 2*C* and Table 2). The bundles showed transverse periodicity of 36.9 nm, roughly corresponding to the crossover distance of the actin filament (35.7 nm) (16). Our observations are generally consistent with a previous study of wild type fascin-actin bundles (17), but contrary to these authors, we found that the transverse pattern occurred at an angle of 63.0 ± 6.23° (Fig. 2*B* and Table 2) and not perpendicular to the bundle axis as they had reported. In agreement with our results, another study of bundles reconstituted with mouse fascin also found 36-nm periodicity with an angle of ~60° to the bundle axis (18). It thus appears that adjacent actin filaments in the fascin-actin bundle are either uniformly rotated or staggered by ~4.1 nm.

TABLE 2
Parameters of wild type fascin-actin bundles

Parameter	This study[a]	Ishikawa *et al.* (17)
No. of filaments in bundle	17 ± 3.9	15 ± 4.7
Bundle width (nm)	142 ± 25	136 ± 44
Distance between filaments[b] (nm)	8.1 ± 0.6	9 ± 0.9
Transverse repeat (nm)	36.9 ± 1.6	36.0
Transverse repeat angle (°)	63.0 ± 6.2	90 (perpendicular to bundle axis)

[a] Values resulting from analysis of 12 or more bundles.
[b] Distance measured between the centers of two neighboring filaments in a raft.

EM analysis further revealed that all the fascin mutants had impaired bundling activity albeit to different extents. Generally, the mutants produced bundles containing fewer and less densely packed filaments than wild type fascin (Fig. 2, *B* and *C*). Consistent with the low speed co-sedimentation assay, mutant 1-4 showed the most dramatic defects, forming thin disordered bundles with fewer than five filaments per bundle. The remaining three mutants exhibited intermediate bundling defects with ~7 filaments per bundle. All the mutants except mutant 2-3 also displayed a statistically significant increase in the average distance between filaments in the bundle. Mutants 1-4 and 1-2 failed to produce the transverse periodicity observed in wild type fascin-actin bundles, an indication that significant changes had occurred in the architecture of their bundles. Mutant 3-4 and to a lesser extent mutant 2-3 showed less severe defects, forming bundles that displayed the characteristic transverse striation albeit not as distinctly and regularly defined as in control bundles. Together, these data showed that despite their varying defects none of the initial fascin mutants had entirely lost the ability to bundle F-actin, which suggested that the main actin-binding sites had not been totally disrupted.

Two Major Actin-binding Sites of Fascin Coincide with Regions of High Sequence Conservation in β-Trefoil Domains 1 and 3—We then attempted to identify the actin-binding sites by amino acid conservation analysis on the surface of the fascin molecule. Indeed, actin is highly conserved throughout evolution, which imposes significant constraints on the conservation of the actin-binding sites of proteins that interact with it. Through analysis of a large number of fascin sequences (supplemental Fig. 5), we determined and plotted the conservation scores of amino acids on the surface of the fascin structure using the program ConSurf (19). This analysis identified two highly conserved regions related by pseudo-2-fold symmetry and wrapping around β-trefoil domains 1 and 3 (Fig. 3*A* and supplemental Movie 1). As above, mutations were introduced

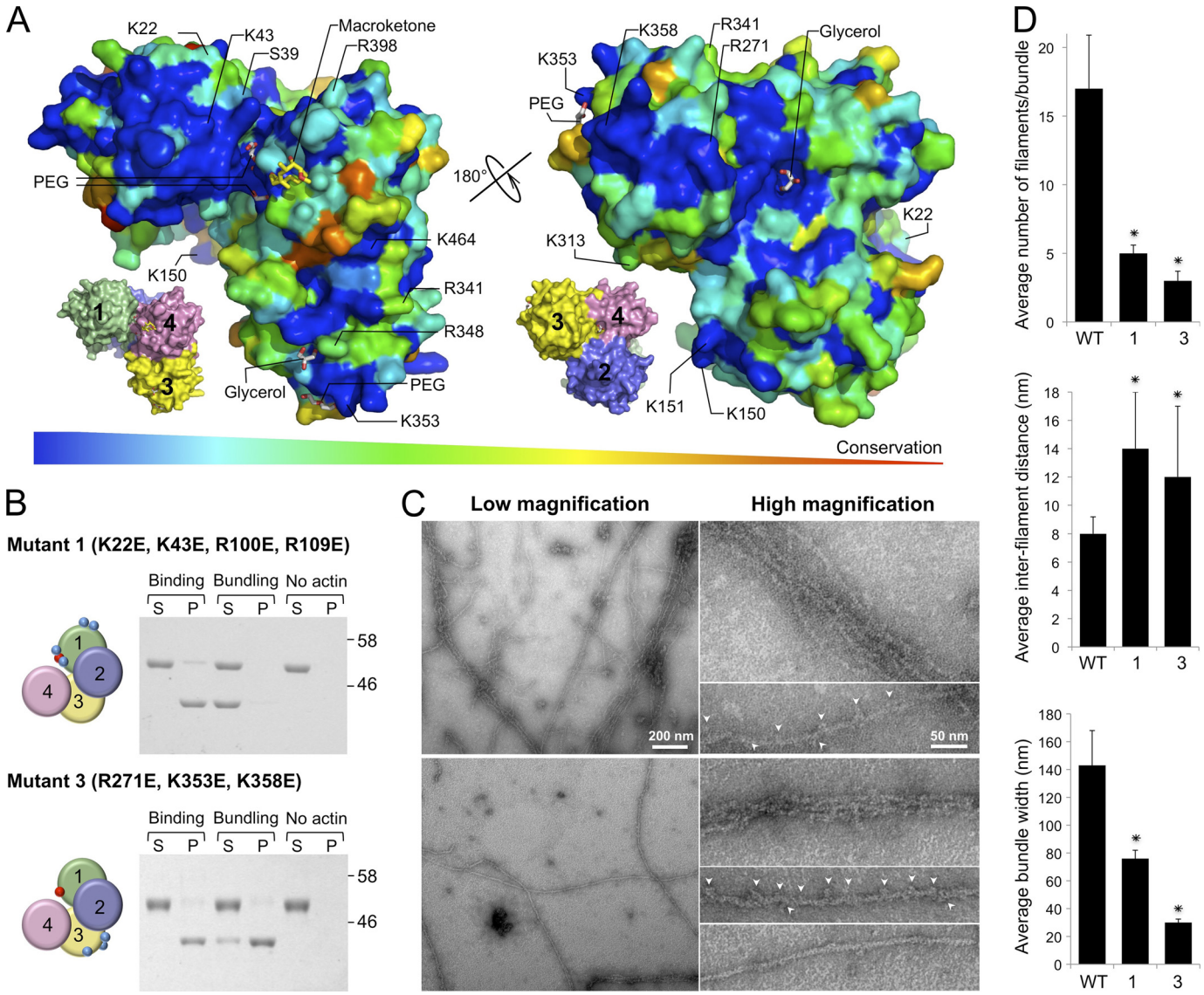

FIGURE 3. **Identification of two major actin-binding sites in β-trefoil domains 1 and 3.** *A*, two views of the surface of the fascin structure rotated by ~180° and colored by residue conservation (conservation decreases from *blue* to *red* as indicated by the *bottom bar*). For reference, small domain-colored diagrams in the same orientation are shown *alongside*. The alignment of fascin sequences used to determine the conservation score of each residue is shown in supplemental Fig. 5. Conservation scores were calculated and displayed with the programs ConSurf (19) and PyMOL (Schrödinger, LLC), respectively. Note that the two largest patches of conserved residues occur in β-trefoil domains 1 and 3. The patch in β-trefoil-1 comprises residue Ser^{39}. The antimetastatic drug macroketone (5) also binds at the edge of this patch (shown, although not part of this structure). In the current structure, molecules of polyethylene glycol and glycerol bind in pockets within the two conserved patches and could guide the design of anticancer drugs. Residues mutated in this study are labeled. *B*, actin binding and bundling assays with fascin mutants 1 and 3 targeting the conserved patches in β-trefoil domains 1 and 3 (conducted as in Fig. 2*A*). *S*, supernatant; *P*, pellet. *C*, transmission electron micrographs of negatively stained actin filaments alone and in the presence fascin mutants 1 and 3 (conducted as in Fig. 2*B*). These mutants have almost completely lost the ability to bundle actin but can bind to the sides of individual actin filaments (*arrowheads*). *D*, quantitative analysis of the bundles formed by mutants 1 and 3 (conducted as in Fig. 2*C*). *Error bars*, S.D.

to perturb these sites (Fig. 3*B*). Mutant 1 (so named because it targeted β-trefoil-1) combined four point mutations adopted from mutants 1-2 and 1-4 that coincidentally displayed the weakest bundling activities among the mutants analyzed above. In high and low speed co-sedimentation assays with F-actin, mutants 1 and 3 (a triple mutant targeting the conserved region in β-trefoil-3) bound actin, but only mutant 3 showed any bundling activity (Fig. 3*B*).

More precise evidence was obtained by EM analysis showing that mutants 1 and 3 recruited only a small fraction of the actin filaments into bundles (Fig. 3, *C* and *D*). Moreover, the few bundles that were observed contained a small number of loosely packed and poorly aligned filaments. Individual actin filaments in both samples frequently showed laterally associated particles (Fig. 3*C*), most likely corresponding to fascin molecules. Combined, these results suggested that the mutations introduced in β-trefoil domains 1 and 3 disrupted one of two major actin-binding sites, whereas the other site was still functional, which would explain the inability of these mutants to form bundles while still binding to the sides of individual filaments.

Based on the EM results, one might have expected to observe less bundling activity for mutant 3 in the low speed co-sedimentation assay (Fig. 3*B*). Note, however, that even the loose bun-

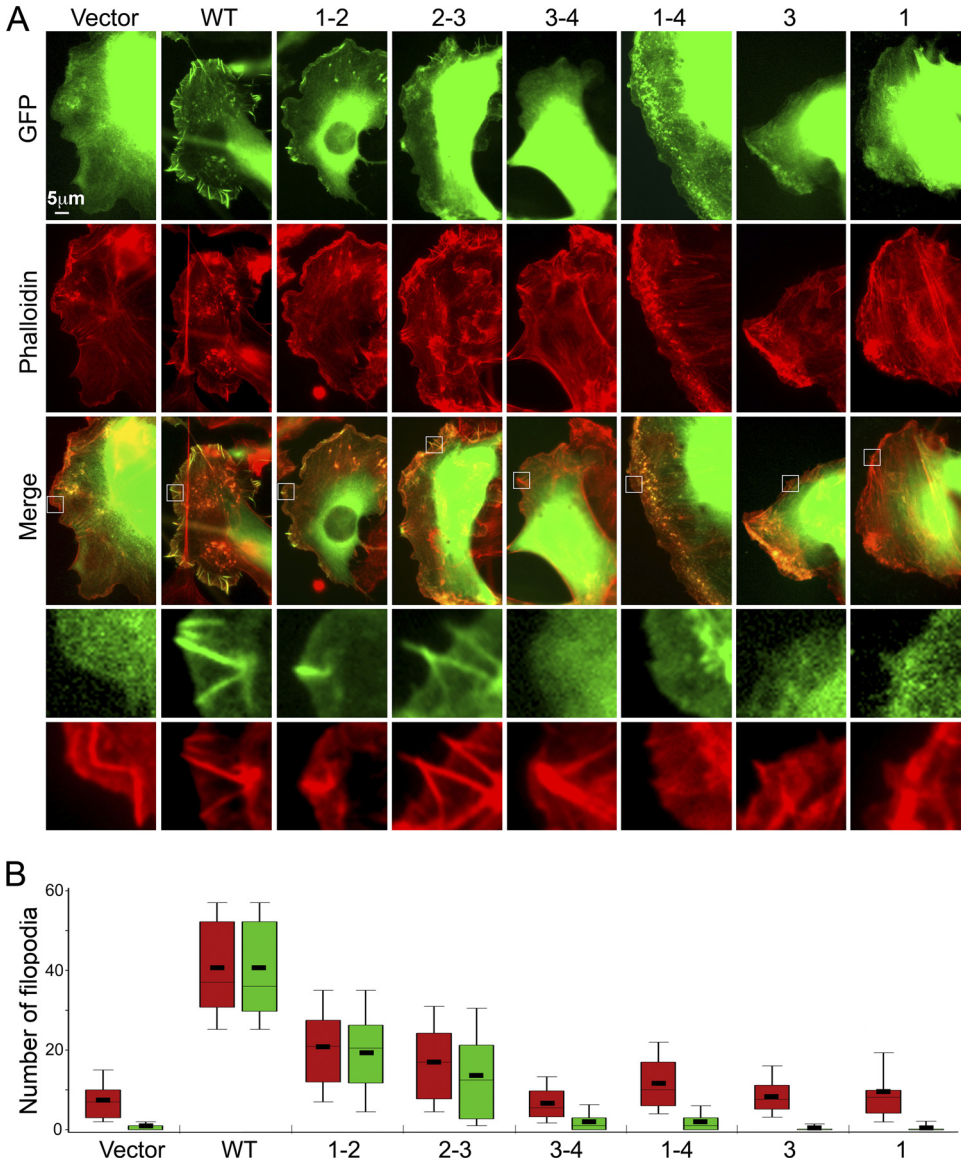

FIGURE 4. **Expression of GFP-fascin mutants in fascin knockdown B16-F1 cells.** *A*, B16-F1 cells co-expressing fascin-shRNA and GFP-fascin constructs (*green*). Cells are co-stained with phalloidin (*red*) to visualize F-actin. The expressed GFP-fascin constructs are indicated at the *top* of each *column* (mutants are named according to Figs. 2 and 3). *Boxed* regions are enlarged at the *bottom* (*scale bar*, 5 μm). *B*, quantitative analysis of the number of filopodia per cell based on phalloidin staining (*red*) or the GFP signal (*green*) for each GFP fusion construct. Data are shown as box-and-whisker plots: *box length* represents values from low to upper quartile, *whiskers* encompass 5th to 95th percentile, *boxes* are divided by the median, and a *bar* represents the mean value (n = 27–36 per construct).

dles formed by mutants 1 and 1-4 (Fig. 2, *A* and *B*) co-sedimented with F-actin when centrifuged for a prolonged time (supplemental Fig. 6). This observation illustrates the susceptibility of the sedimentation assay to small changes in experimental conditions and confirms that definitive conclusions about the bundling activity of the mutants can only be drawn after additional analysis by EM.

Cellular Phenotypes of Fascin Mutants—To test the cellular effects of the fascin mutants, knockdown and rescue experiments were performed in mouse melanoma B16-F1 cells (Fig. 4). As shown previously (13), shRNA depletion of endogenous fascin dramatically decreases the number of filopodia in these cells. Using this system, we attempted to rescue formation of filopodia by co-expressing GFP-tagged fascin mutants in cells co-expressing fascin shRNA. In control knockdown cells co-expressing a GFP vector, we observed very few filopodia, which were typically buckled near the cell edge, which is consistent with previous observations (3). Moreover, these filopodia could only be detected by actin staining with phalloidin as they did not accumulate the GFP fluorescence marker. The co-expression of wild type GFP-fascin resulted in a ~3-fold increase in the number of GFP-fascin-enriched filopodia compared with control cells. The co-expression with fascin mutants revealed that all the mutants were deficient in their ability to rescue formation of filopodia and to localize to filopodial bundles albeit to different extents. Thus, mutants 1-2 and 2-3 retained some activity, producing a slight increase in the number of filopodia and showing some enrichment in filopodia compared with control cells. Mutants 3-4, 1-4, 1, and 3 were unable to rescue

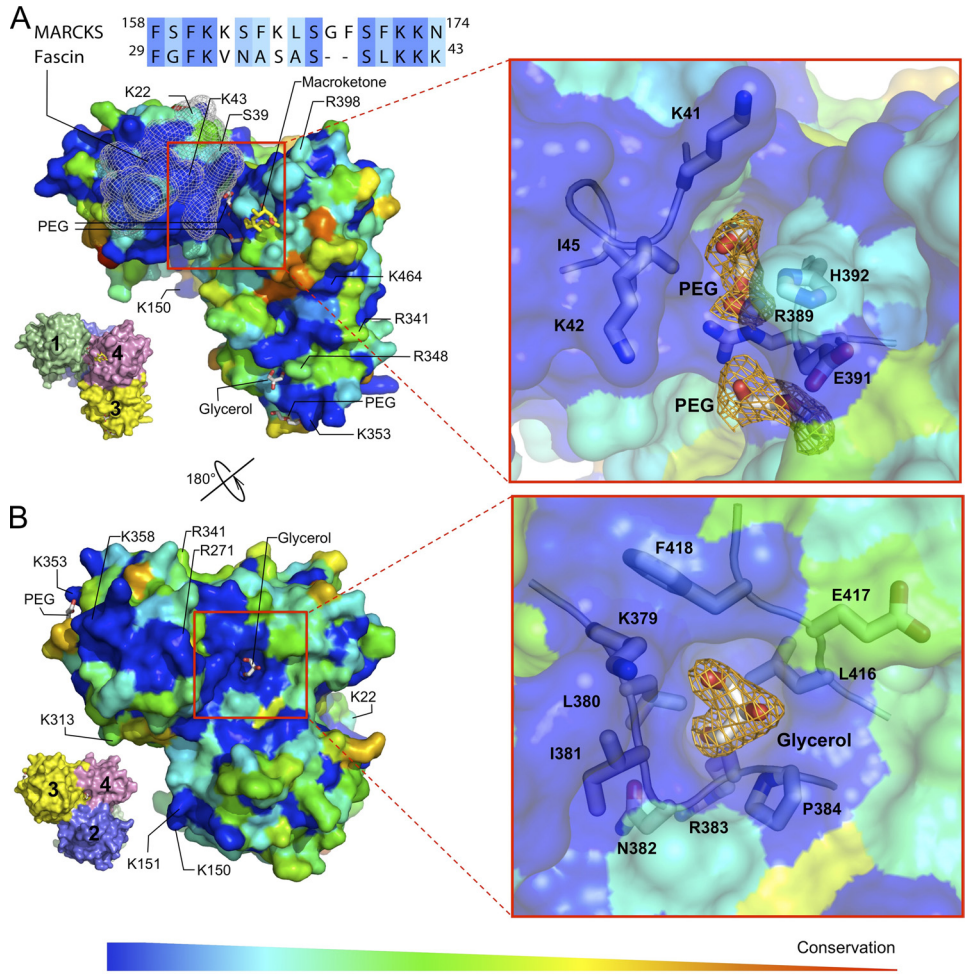

FIGURE 5. **Molecules of glycerol and PEG bound in pockets within the two major actin-binding sites of fascin.** *A*, surface representation of the actin-binding site in β-trefoil-1 colored by residue conservation (*left*) and an enlarged view (*right*) showing molecules of PEG bound in the cleft formed at the interface between β-trefoil domains 1 and 4 (see also supplemental Movie 1). Residue conservation decreases from *blue* to *red* as indicated by the *bar* at the *bottom* of the figure. Note that the actin-binding site in β-trefoil-1 includes the MARCKS-related sequence (fascin residues 29–43; indicated by a *mesh surface*) and residue Ser[39] (labeled), which have been implicated in actin binding (7, 8). An alignment of the sequences of human fascin (UniProt accession number Q16658) and MARCKS (UniProt accession number P29966) is shown for this region (identity, *dark blue*; conservation, different shades of *cyan*). *B*, surface representation of the actin-binding site in β-trefoil-3 (*left*) and an enlarged view (*right*) of a molecule of glycerol bound in a pocket formed at the interface between β-trefoil domains 2, 3, and 4. The two actin-binding sites are related by pseudo-2-fold symmetry as indicated. Also shown are some of the amino acids that form the binding pockets for the molecules of PEG and glycerol as well as the $2F_o - F_c$ electron density map contoured at 1.0 σ around these molecules. Shown *alongside* are small domain-colored diagrams of the fascin structure in the same orientation.

formation of filopodia. These four mutants also failed to localize to the few remaining filopodia detected by phalloidin staining and instead appeared to be evenly distributed throughout the cytoplasm.

DISCUSSION

Actin bundling proteins present at least two actin-binding sites, which is commonly accomplished through dimerization as is the case with the prototypical actin-bundling protein α-actinin (20). However, some actin bundling proteins, such as fimbrin (21), are monomeric but display internal pseudosymmetry and thus bind actin through two structurally related but different sites. As we have shown here, fascin belongs to the latter category. Collectively, our results suggest that fascin contains two major actin-binding sites located within β-trefoil domains 1 and 3 and related by pseudo-2-fold symmetry. Some evidence already implicated the site identified here in β-trefoil-1 in actin binding, including its proximity to the binding site of the fascin inhibitor macroketone (5) and the presence within this region of Ser[39] that when phosphorylated by PKC inhibits F-actin bundling by fascin (7). This area also includes residues 29–43 that had been postulated to participate in actin binding based on limited sequence similarity with an actin-binding site in MARCKS (8). The identification here of the actin-binding site in β-trefoil-1 was based on entirely different criteria, notably sequence conservation on the surface of a crystal structure of fascin in which all the loops could be visualized. This method also resulted in the identification of a novel actin-binding site in β-trefoil domain 3. Corroborating the results of the bioinformatics analysis, mutations of residues in both conserved surfaces (mutants 1 and 3) impaired bundle formation *in vitro* and formation of filopodia in cells. Mutant 1-4, which also displayed severe F-actin bundling defects, partially overlaps with mutant 1. Particularly, residues Lys[22] and Lys[43], which were substituted in both mutants, fall near the regulatory residue Ser[39] and form part of the MARCKS-related sequence (Fig. 5*A*), providing

strong experimental support for the involvement of this sequence in actin binding.

Mutations outside the two major conserved regions generally had a milder phenotype *in vitro* and in cells. However, although the *in vitro* and cellular results were generally in good agreement, mutant 3-4 showed significant bundling activity *in vitro* but had no activity in cells. Certain discrepancies between the two sets of data were not totally unexpected because some of the mutations may affect interactions with proteins other than actin in cells. For instance, fascin is known to interact with β-catenin (22) and was recently shown to also interact with Rab35 (23). The latter interaction was proposed to play an important role in recruiting fascin to filopodia. However, the binding sites of β-catenin and Rab35 on fascin are still unknown. It is thus likely that some of the mutations studied here, which cover almost the entire surface of the fascin molecule, affect the interactions of fascin with β-catenin, Rab35, and other binding partners of fascin in cells of which little is still known (1).

The bundling defects produced by mutations outside the two major actin-binding sites also suggest that fascin makes secondary contacts in the three-dimensional bundle; *i.e.* each fascin molecule might interact with more than two filaments in the bundle. This appears a likely possibility because the bundles are tightly packed with an average apparent distance between filaments of ~8.1 nm, and the fascin molecule has a high degree of internal symmetry and similar dimensions (~5–6 nm) in most directions. The observed distance between filaments in the bundle seems surprisingly small given the dimensions of the fascin molecule and those of the actin filament whose thickness oscillates between ~6 and ~10 nm along the longitudinal axis (24). Most likely, fascin binds at the interface between actin subunits in the filament, a location where most actin-binding proteins bind (25, 26), bridging the narrow area of neighboring filaments. Another observation made here is that the transverse periodicity in wild type fascin-actin bundles occurs at an angle of ~63.0°, which is in agreement with a study of reconstituted bundles formed by mouse fascin (18) but disagrees with another study that found that the repeat is perpendicular to the bundle axis (17). Our results thus suggest that neighboring filaments in the bundle are either uniformly rotated or staggered by ~4.1 nm, which could help accommodate fascin molecules in the tight bundle. Although the goal of our EM analysis was to compare bundles formed by wild type and mutant fascin under reported conditions (17, 18), it remains unclear how fascin constrains F-actin into such a tight bundle and what is the exact position and conformation of fascin in the bundle. These observations underscore the need for future high resolution studies of the bundle using cryo-EM tomography.

The conserved surface of β-trefoil-1 extends slightly into β-trefoil-4 and that of β-trefoil-3 extends into β-trefoil-2 (Fig. 3*A*), such that the actin-binding sites might slightly straddle these adjacent domains. This probably explains why the binding of macroketone in β-trefoil-4 at the edge of the conserved surface, interferes with the formation of filopodia. In this regard, the crystal structure determined here provides one additional important clue; molecules of glycerol and polyethylene glycol are bound in pockets and clefts formed at the interface between domains within the two major actin-binding sites (Fig. 5). Particularly, the molecules of polyethylene glycol bound in the cleft formed at the interface between β-trefoil domains 1 and 4 are positioned halfway between the macroketone-binding site and Ser^{39} and the MARCKS-related sequence (Fig. 5*A*). These molecules seem to be tightly bound, and their pockets appear better suited for small molecule recognition than that of macroketone, which looks loosely bound on the surface of the fascin molecule. These molecules of glycerol and polyethylene glycol could therefore guide the rational design of new fascin inhibitors to be used as anticancer agents.

Acknowledgments—We thank Farida Korobova for help with the expression of fascin mutants in cells. Use of the Industrial Macromolecular Crystallography Association Collaborative Access Team beamline 17-ID was supported by the Industrial Macromolecular Crystallography Association through a contract with the Hauptman-Woodward Medical Research Institute. The Advanced Photon Source was supported by United States Department of Energy Contract W-31-109-Eng-38. The transmission electron microscope was supported by National Institutes of Health Shared Instrumentation Grant S10 RR-22482 (to T. S.).

REFERENCES

1. Machesky, L. M., and Li, A. (2010) *Commun. Integr. Biol.* **3,** 263–270
2. Li, A., Dawson, J. C., Forero-Vargas, M., Spence, H. J., Yu, X., König, I., Anderson, K., and Machesky, L. M. (2010) *Curr. Biol.* **20,** 339–345
3. Vignjevic, D., Kojima, S., Aratyn, Y., Danciu, O., Svitkina, T., and Borisy, G. G. (2006) *J. Cell Biol.* **174,** 863–875
4. Hashimoto, Y., Skacel, M., and Adams, J. C. (2005) *Int. J. Biochem. Cell Biol.* **37,** 1787–1804
5. Chen, L., Yang, S., Jakoncic, J., Zhang, J. J., and Huang, X. Y. (2010) *Nature* **464,** 1062–1066
6. Sedeh, R. S., Fedorov, A. A., Fedorov, E. V., Ono, S., Matsumura, F., Almo, S. C., and Bathe, M. (2010) *J. Mol. Biol.* **400,** 589–604
7. Ono, S., Yamakita, Y., Yamashiro, S., Matsudaira, P. T., Gnarra, J. R., Obinata, T., and Matsumura, F. (1997) *J. Biol. Chem.* **272,** 2527–2533
8. Mosialos, G., Yamashiro, S., Baughman, R. W., Matsudaira, P., Vara, L., Matsumura, F., Kieff, E., and Birkenbach, M. (1994) *J. Virol.* **68,** 7320–7328
9. Yamashiro-Matsumura, S., and Matsumura, F. (1985) *J. Biol. Chem.* **260,** 5087–5097
10. Cant, K., and Cooley, L. (1996) *Genetics* **143,** 249–258
11. Graceffa, P., and Dominguez, R. (2003) *J. Biol. Chem.* **278,** 34172–34180
12. Adams, P. D., Afonine, P. V., Bunkóczi, G., Chen, V. B., Davis, I. W., Echols, N., Headd, J. J., Hung, L. W., Kapral, G. J., Grosse-Kunstleve, R. W., McCoy, A. J., Moriarty, N. W., Oeffner, R., Read, R. J., Richardson, D. C., Richardson, J. S., Terwilliger, T. C., and Zwart, P. H. (2010) *Acta Crystallogr. D Biol. Crystallogr.* **66,** 213–221
13. Emsley, P., Lohkamp, B., Scott, W. G., and Cowtan, K. (2010) *Acta Crystallogr. D Biol. Crystallogr.* **66,** 486–501
14. Sukow, C., and DeRosier, D. (1998) *J. Mol. Biol.* **284,** 1039–1050
15. Yang, C., Czech, L., Gerboth, S., Kojima, S., Scita, G., and Svitkina, T. (2007) *PLoS Biol.* **5,** e317
16. Holmes, K. C. (2009) *Nature* **457,** 389–390
17. Ishikawa, R., Sakamoto, T., Ando, T., Higashi-Fujime, S., and Kohama, K. (2003) *J. Neurochem.* **87,** 676–685
18. Edwards, R. A., Herrera-Sosa, H., Otto, J., and Bryan, J. (1995) *J. Biol. Chem.* **270,** 10764–10770
19. Ashkenazy, H., Erez, E., Martz, E., Pupko, T., and Ben-Tal, N. (2010) *Nu-*

cleic Acids Res. **38,** (suppl.) W529–W533
20. Broderick, M. J., and Winder, S. J. (2005) *Adv. Protein Chem.* **70,** 203–246
21. Galkin, V. E., Orlova, A., Cherepanova, O., Lebart, M. C., and Egelman, E. H. (2008) *Proc. Natl. Acad. Sci. U.S.A.* **105,** 1494–1498
22. Tao, Y. S., Edwards, R. A., Tubb, B., Wang, S., Bryan, J., and McCrea, P. D. (1996) *J. Cell Biol.* **134,** 1271–1281
23. Zhang, J., Fonovic, M., Suyama, K., Bogyo, M., and Scott, M. P. (2009) *Science* **325,** 1250–1254
24. Fujii, T., Iwane, A. H., Yanagida, T., and Namba, K. (2010) *Nature* **467,** 724–728
25. Dominguez, R. (2004) *Trends Biochem. Sci.* **29,** 572–578
26. Dominguez, R., and Holmes, K. C. (2011) *Annu. Rev. Biophys.* **40,** 169- 186